# Numerical Analysis of Solidification in a Thick-Walled Cylindrical Container

Richard N. Smith,* Richard L. Pike,† and Carol M. Bergs‡
*Rensselaer Polytechnic Institute, Troy, New York*

**A numerical analysis has been conducted to investigate the process of axisymmetric, diffusion-controlled solidification in a thick-walled cylindrical container using an alternating-direction-implicit method to solve a nondimensionalized enthalpy formulation of the governing two-dimensional equations. The effects of wall thickness, thermal properties, initial wall temperature distribution, and container aspect ratio on the freezing process are examined. The complex interaction between these parameters and the external cooling conditions leads to some interesting conclusions concerning casting solidification, particularly when external heat removal rates are low.**

## Nomenclature

$A, B$ = coefficients in discretization equation (9)
$c$ = heat capacity, J/kg °C
$\hat{c}$ = ratio of PCM liquid to solid heat capacity
$Fo$ = Fourier number, dimensionless time
$G$ = ratio of container radius to height
$h$ = specific enthalpy, J/kg
$k$ = thermal conductivity, W/m °C
$\bar{k}$ = ratio of wall to PCM solid thermal conductivity
PCM = phase change material
$Q$ = energy content, J
$\bar{Q}$ = dimensionless energy content
$r$ = dimensionless radial coordinate
$\Delta r$ = dimensionless radial node separation
$R$ = overall container radius, m
$R_w$ = container sidewall thickness, m
$\bar{R}$ = ratio of sidewall thickness to overall radius
$Ste$ = Stefan number
$t$ = time, s
$T$ = temperature, °C
$T_w$ = exterior wall $T$ applied as boundary condition
$V$ = volume of PCM, m$^3$
$\bar{V}$ = dimensionless PCM volume
$z$ = dimensionless vertical coordinate, m
$\Delta z$ = dimensionless vertical node separation
$Z$ = overall container height, m
$Z_w$ = container base thickness, m
$\bar{Z}$ = ratio of base thickness to overall height
$\alpha$ = thermal diffusivity, m$^2$/s
$\bar{\alpha}$ = ratio of wall to PCM solid diffusivity
$\gamma$ = radial coordinate, m
$\zeta$ = vertical coordinate, m
$\theta$ = dimensionless enthalpy
$\lambda$ = PCM solid-liquid heat, J/kg
$\rho$ = density, kg$^2$/m$^3$
$\varphi$ = dimensionless temperature

*Subscripts*

$fr$ = saturation conditions
$L$ = PCM liquid phase
N, S, E, W = node above, below, to the right of, and to the left of control volume, respectively
P = node in center of control volume
$w$ = wall conditions or properties
Note: No subscript refers to PCM solid phase.

*Superscripts*

$k$ = time-step number
0 = initial conditions

## Introduction

HEAT-TRANSFER problems involving solid/liquid phase change comprise a long-standing research area. Applications such as thermal energy storage, metal casting, welding, nuclear reactor safety, advanced food processing, and cryosurgery have all generated continued interest in the subject, as evidenced by numerous regular contributions to the technical literature. Recent extensive reviews of the area have described analytical and numerical methods for solving such problems.[1-3]

The problem of interest to this paper is that of a thick-walled cylinder inside which a phase change process occurs. An example is a two-chambered crucible/mode assembly (Fig. 1) that is inserted into an induction furnace. Solid material within the upper chamber is melted, at which point it is allowed to drain into the lower mold chamber, and then cooled to begin solidification. Since the mold is connected to the crucible during the heating operation, it attains a temperature distribution which can have a profound effect on the ensuing solidification process.

The manner in which solidification takes place may depend more on the thermal properties of the mold and its initial temperature distribution than on the nature of any imposed external cooling conditions. The material properties of the resulting solid can be integrally related to the rate and direction of propagation of the phase front, as can the nature of void formation, for materials having different solid and liquid phase densities.

By preheating (or cooling) a mold in a prescribed manner, or by designing a mold with a prescribed distribution of wall thickness, it should be possible to control the solidification process. However, in two and three dimensions, little experimental or analytical information is available to provide guidelines for such control or even to provide a good understanding of how a thick boundary interacts with a liquid/solid phase change phenomenon.

Some results are available, however, for one-dimensional problems. An exact solution for freezing of a semi-infinite superheated liquid adjacent to a semi-infinite precooled slab of finite heat capacity and thermal conductivity is described by Carslaw and Jeager.[4] Siegel and Savino[5] used an implicit integration, while Epstein[6] and El-Genk and Cronenberg[7,8]

Presented as Paper 85-1044 at the AIAA 20th Thermophysics Conference, Williamsburg, VA, June 19–21, 1985; received July 13, 1985; revision received Jan. 18, 1986. 

*Associate Professor, Department of Mechanical Engineering, Aeronautical Engineering, and Mechanics.

†Graduate Research Assistant, Department of Mechanical Engineering, Aeronautical Engineering, and Mechanics. Presently at Northern Research and Engineering Company, Woburn, MA.

‡Graduate Research Assistant, Department of Mechanical Engineering, Aeronautical Engineering, and Mechanics.

applied an integral method to the coupled heat-transfer problems of solidification adjacent to a semi-infinite or finite thickness cooled plate. In each case, the superheated liquid phase was infinite in extent and flowing by forced convection so that a constant heat-transfer rate was provided to the frozen layer from the liquid phase (heat-transfer coefficient assumed known). This heat flux plus the latent heat of fusion are conducted away from the solid layer into the wall. Under these conditions, the frozen layer grows in extent until the thermal capacity of the boundary wall is depleted and its internal resistance limits the conduction rate; then the frozen layer begins to remelt. Analogous problems may be contrived whereby the solid layer reaches an asymptotic thickness, after which no further phase change occurs, or where the growth of the solid layer continues, but more and more slowly.

With respect to a casting process, one could imagine that the inward solidification rate would be significantly slowed with a thick mold wall, and, with sufficient superheat in the liquid, even some remelting could occur. A casting process could potentially be designed, for example, so that the solidification could be controlled directionally (e.g., from bottom to top in a cylindrical ingot, rather than radially inward).

The purpose of the present paper is to study a simple cylindrical casting problem, similar to the one described above. The effects of the wall geometry and thermophysical properties on the rate of solidification, phase front shape, and temperature distribution for a cylindrical geometry have been determined.

The numerical procedure is based on an enthalpy formulation[9] used by Smith and Koch[10] to study freezing adjacent to finned surfaces. The method has been revised recently by Boucheron and Smith[11] to permit solution of a wider variety of similar problems. A similar problem of conjugate transport in a freezing solid and its two-dimensional, rectangular, thin-walled container was studied by Schneider.[12]

## Analysis

The problem under consideration is shown in Fig. 2. A cylindrical container of outer radius $R$, wall thickness $R_w$, height $Z$, base thickness $Z_w$, and a specified initial temperature distribution is filled with a liquid phase change material (PCM) at a uniform initial temperature. At time equal to zero an external cooling condition on the outer wall is imposed so that cooling of the PCM and subsequent solidification begin.

The initial temperature distribution of the container has a strong influence on the subsequent heat-transfer process. If the wall is initially colder than the PCM melting temperature (e.g., the PCM is poured into a cold mold), then heat will be removed more quickly from the PCM and solidification will begin at once. If the wall is initially at the phase change temperature (or above), then the freezing process will be retarded. If there are initially large thermal gradients in the container, then the relative influence of heat transfer from the base and side may be altered.

In the present analysis, three different initial wall temperature distributions have been considered. The first is a uniformly subcooled wall; the second is a wall uniformly heated to the initial PCM temperature (e.g., the fusion temperature); and the third is an imposed temperature gradient in the wall; with the top of the sidewall at the PCM initial temperature, the base is subcooled and the sidewall temperature increases linearly from top to bottom.

Two different external cooling conditions have been considered. An isothermal, subcooled outer wall temperature ($r = R$, $z = 0$) corresponds to the limiting case of a very high external cooling condition; while an adiabatic outer wall corresponds to the "opposite" limiting condition of no external heat loss. In that case, all solidification is derived from the initial wall subcooling.

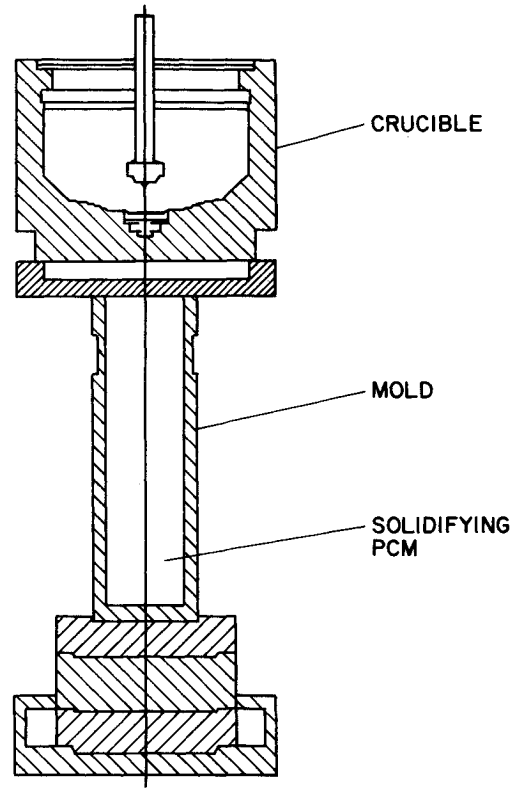


Fig. 1 Example crucible mold assembly.

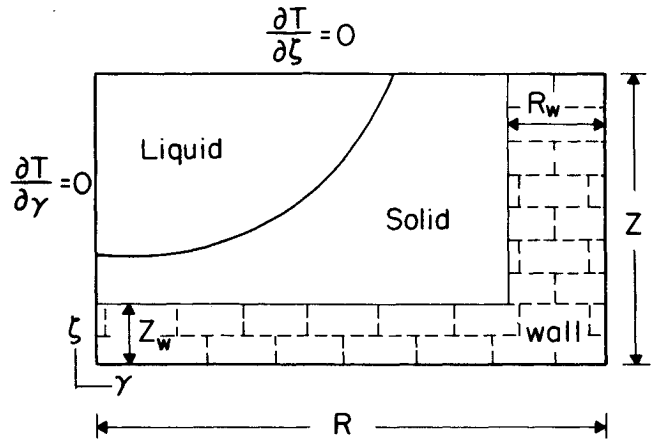


Fig. 2 Container geometry.

The problem formulation presented here neglects natural convection in the liquid phase. Since the specific cases discussed include no liquid phase superheat, this assumption does not introduce any error. Were liquid superheat present, the effect would be a retarding of solidification but an increase in heat transfer from the PCM relative to the pure diffusion case. However, some evidence suggests that natural convection effects for inward solidification are not significant.[13]

## Formulation of Governing Equations

In what follows, thermal conductivity and specific heat are assumed constant in each region. The energy equation in cylindrical coordinates for axisymmetric conduction is

$$\rho \frac{\partial h}{\partial t} = \frac{k}{\gamma} \frac{\partial}{\partial \gamma}\left(\gamma \frac{\partial T}{\partial \gamma}\right) + k \frac{\partial^2 T}{\partial \zeta^2} \tag{1}$$

This equation applies to both the PCM and wall regions; the only differences are in the relationship between temperature and enthalpy and in the property values.

The wall temperature-vs-enthalpy relationship is given by

$$h = c_w T \tag{2}$$

The temperature-enthalpy relationship for the PCM is more complicated:

In the solid region:

$$T < T_{fr} \text{ and } h = cT \tag{3a}$$

In the transition region:

$$T = T_{fr} \text{ and } cT_{fr} \le h \le \lambda + cT_{fr} \tag{3b}$$

In the liquid region:

$$T > T_{fr} \text{ and } h = \lambda + cT_{fr} + c_L(T - T_{fr}) \tag{3c}$$

The following dimensionless parameters are defined as

$$\bar{G} = R/Z; \quad r = \gamma/R; \quad z = \zeta/R = \zeta/Z\bar{G}$$

$$\theta = \frac{h - h_{fr}}{\lambda}; \quad \varphi = \frac{T - T_{fr}}{\lambda/c}; \quad Ste = \frac{T_{fr} - T_{\text{ref}}}{\lambda/c}$$

$$Fo = kt/\rho c R^2; \quad \bar{\alpha} = \alpha_w/\alpha; \quad \bar{k} = k_w/k$$

$$\hat{c} = c/c_L; \quad \bar{R} = R_w/R; \quad \bar{Z} = Z_w/Z \tag{4}$$

Substitution of these into Eq. (1) yields

$$\frac{\partial \theta}{\partial Fo} = \nabla^2 \varphi \tag{5}$$

Nondimensionalizing the PCM temperature-enthalpy relations by the use of Eq. (4) results in

$$\varphi < 0, \quad \theta = \varphi \quad \text{solid region} \tag{6a}$$

$$\varphi = 0, \quad 0 \le \theta \le 1 \quad \text{fusion point} \tag{6b}$$

$$\varphi > 0, \quad \theta = 1 + (\varphi/\hat{c}) \quad \text{liquid region} \tag{6c}$$

Within the wall region, the conduction equation becomes

$$\frac{\partial \varphi}{\partial Fo} = \bar{\alpha} \nabla^2 \varphi \tag{7}$$

Thus, the effect of this nondimensionalization is to change the solution from

$$h(\gamma, \zeta, t) \quad \text{and} \quad T(\gamma, \zeta, t)$$

depending on $[R, Z, R_w, Z_w, \lambda, \rho, \rho_w, c, c_L, c_w, k, k_w, T_{fr}, T_w, h_{fr}]$, to

$$\theta(r, z, Fo) \quad \text{and} \quad \varphi(r, z, Fo)$$

depending on $[\bar{G}, \bar{R}, \bar{Z}, \hat{c}, \bar{\alpha}, \bar{k}, Ste]$. When the exterior boundary conditions are nondimensionalized, they become

Type I (isothermal outer wall):

$$T = T_w \text{ becomes } \varphi = -Ste \tag{8a}$$

Type II (adiabatic outer wall):

$$\frac{\partial T}{\partial n} = 0 \text{ becomes } \frac{\partial \varphi}{\partial n} = 0 \tag{8b}$$

where $n$ represents either $z$ at the base or $r$ at the side. Symmetry conditions along $r = 0$ and $z = 1/\bar{G}$ are also imposed, so that $\partial T/\partial n = 0$ there. Figure 3 shows the dimensionless geometry.

## Numerical Solution

The governing equations have been converted into a system of finite-difference equations by discretizing the domain and applying the governing equations for conservation of energy to each of the resulting control volumes. Figure 4 shows the finite-difference grid that was used. A uniform node spacing was imposed in each of the "quadrants" indicated in the figure.

Only the rudiments of the numerical procedure will be presented here. The details are available in Ref. 14, and the reader is also referred to Refs. 10 and 11 for additional examples.

If the subscript P refers to a node on which an energy balance is being made, N, S, E, W refer to surrounding nodes, and superscripts $k$ and $k-1$ refer to the current and previous time steps, respectively, then the general finite-difference equation takes the following fully implicit form:

$$\frac{\theta_P^k - \theta_P^{k-1}}{\Delta Fo} = \left(A_N \varphi_N^k + A_P \varphi_P^k + A_S \varphi_S^k\right) + \left(B_E \varphi_E^k + B_P \varphi_P^k + B_W \varphi_W^K\right) \tag{9}$$

The values of the coefficients on the right-hand side of Eq. (9) depend upon the location within the domain and the discretization parameters.

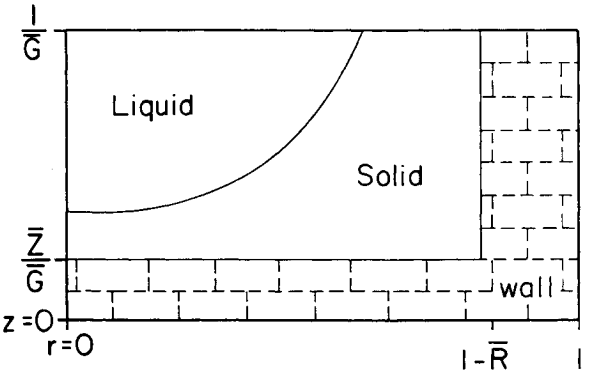


Fig. 3 Dimensionless geometry.

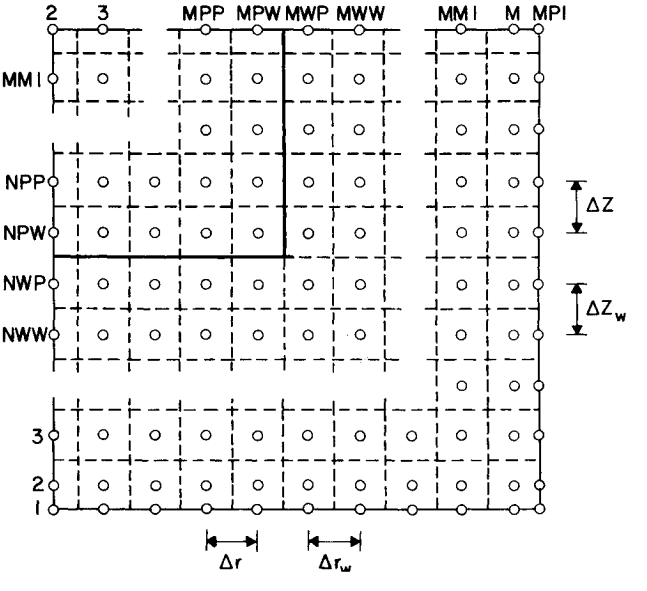


Fig. 4 Discretization grid.

To utilize standard solution routines for the values of $\theta_P^k$ for all points in the PCM domain, Eq. (9) must be modified so that the right-hand side contains $\theta_N^k$, $\theta_P^k$, $\theta_S^k$,... rather than $\varphi_N^k$, $\varphi_P^k$, $\varphi_S^k$,.... This has been done by assuming that the relations between $\theta_N^k$ and $\varphi_N^k$, $\theta_P^k$ and $\varphi_P^k$, etc., are the same at the current time step as they were at the previous time step [Eqs. (6)]. For example, if at time $k-1$, $\varphi_N^{k-1}=0$, then $A_N$ is set to zero, and $\varphi_N^k$ is replaced by $\theta_n^k$ in Eq. (9). If $\varphi_N^{k-1}<0$, then $A_n$ is unaltered and $\varphi_N^k$ is replaced by $\theta_N^k$ in Eq. (9). If $\varphi_N^{k-1}>0$, then $A_N$ is set to $\hat{c}A_N$, $\varphi_N^k$ is replaced by $\theta_N^k$ and a constant equal to $-\hat{c}$ is added to Eq. (9). The constant is later incorporated into a "lumped constant" term for calculation of dimensional nodal enthalpies. The resulting finite-difference equation takes the form

$$\frac{\theta_P^k-\theta_P^{k-1}}{\Delta Fo}=\left(A'_N\theta_N^k+A'_P\theta_P^k+A'_S\theta_S^k\right)+\left(B'_E\theta_E^k+B'_P\theta_P^k+B'_W\theta_W^k\right)+C'_P \tag{9a}$$

Because the values of $A'_N, A'_P,\ldots$ depend on the values of the dimensionless temperature at the previous time step $(k-1)$, an iteration on the values of the coefficients is necessary. Since these coefficients have distinct values which depend only on the phase of the nodes, only a single iteration is required. A similar procedure has been described by Schneider and Raw.[15]

Of course, in the wall region there is only one phase, so that the procedure described above is not necessary, since $\theta=\varphi$ for all nodes.

An alternating-direction-implicit (ADI) inversion scheme was used to solve the set of equations (9a) for the distribution of $\theta_P^k$ values.[16] A variety of dimensionless node spacings were utilized according to the geometric parameter values of a problem, but typically a $20\times 60$ node grid was found to be adequate. An automatic time-step adjustment routine was also implemented to keep the maximum enthalpy change within the domain to between 2 and 5% of the value at the previous time step.

Accuracy of the procedures was assessed by computing temperature fields with no phase change occurring and comparing to known exact solutions. Also, the results for freezing within an isothermal-wall enclosure were compared with earlier results[10] to verify consistency of the method for phase change problems.

All computations and plots were obtained using an IBM 4341 computer in Rensselaer Polytechnic Institute's Center for Interactive Computer Graphics.

## Results and Discussion

The fundamental result of this computation is the array of nodal enthalpy values at each time step. From this the PCM and wall energy contents, PCM fraction frozen, approximate phase front locations, and nodal temperatures may be determined by straightforward calculations. For example, the fraction frozen is simply the portion of the PCM volume having $\theta<0$. For nodes having $0<\theta<1$, the fraction of the node that is frozen is taken to be $1-\theta$. The phase front profile is given by the locus of all nodes having dimensionless enthalpy between 0 and 1. In addition, from the nodal temperature arrays, the heat fluxes at the outer wall and PCM wall interface may also be obtained.

To examine individually the effects of the various parameters and conditions on the freezing process, a baseline case has been defined for a comparison with all other runs. The parameters and conditions that comprise this case are: $\bar{Z}=0.333$, $\bar{k}=2.00$, $\bar{G}=0.10$, $\theta^\circ=1.00$; $\bar{R}=0.333$, $\bar{\alpha}=2.00$, $Ste=1.00$, $\hat{c}=1.20$; exterior boundary condition: type I, $\varphi=-1.00$; initial PCM, $\varphi=0.00$; and initial wall, $\varphi=-1.00$. This case corresponds to a container whose height is 10 times its radius, with sidewall thickness of one-third of the total radius and bottom wall thickness of one-third of the total height. Material properties are approximately those of uranium solidifying in a graphite mold. The liquid phase is initially at the phase change temperature, the wall is initially subcooled, and the outer wall surface is maintained at the subcooled temperature.

The parameters chosen to represent the freezing behavior are the fraction frozen and the integrated energy content as functions of time. Also, plots of representative phase front profiles have been obtained. Instantaneous heat-transfer rates do not yield significant information over that presented here, and so are not included.

A wall having a high value of thermal conductivity should result in a more rapid freezing rate. This is illustrated in Fig. 5, in which fraction frozen and dimensionless energy content are plotted for four values of $\bar{k}$, including the baseline value of 2.0. Only a small increase in freezing rate occurs as $\bar{k}$ is increased to 3.0, but a poorly conducting wall results in significantly longer solidification times.

The values of $\bar{Q}$ in this and subsequent figures represent the PCM energy normalized by the latent plus sensible initial energy content of the PCM. Therefore, even though the fraction frozen approaches 1, $\bar{Q}$ remains nonzero since a value of zero would represent removal of all sensible energy from the solid PCM so that its temperature becomes equal to the outer wall temperature (or to the initial wall temperature, for a type II external cooling condition).

The curves of fraction frozen (FF) show a slight waviness (which has been removed from these figures), while those of $\bar{Q}$ appear quite smooth. This was unexpected since both quantities are determined from the enthalpy field calculated numerically. However, $\bar{Q}$ represents latent plus sensible energy content of the PCM, while FF represents only the latent energy. The finite domain discretization results in a slight oscillation of local freezing rates. The oscillation is removed when a finer mesh is utilized, although the FF results fall directly on top of the curves shown in Fig. 5. The inclusion of sensible energy in $\bar{Q}$ assures a smooth variation. It should be emphasized that $\bar{Q}$ is a more direct result of the actual numerical computation since the values of the nodal enthalpies are the fundamental result of that computation. Fraction frozen or phase front profiles are determined somewhat artificially and are not used in any way in subsequent time-step calculations. However, since fraction frozen and phase front propagation are the more visible results of a solidification process, they are the aspects emphasized in the present discussion.

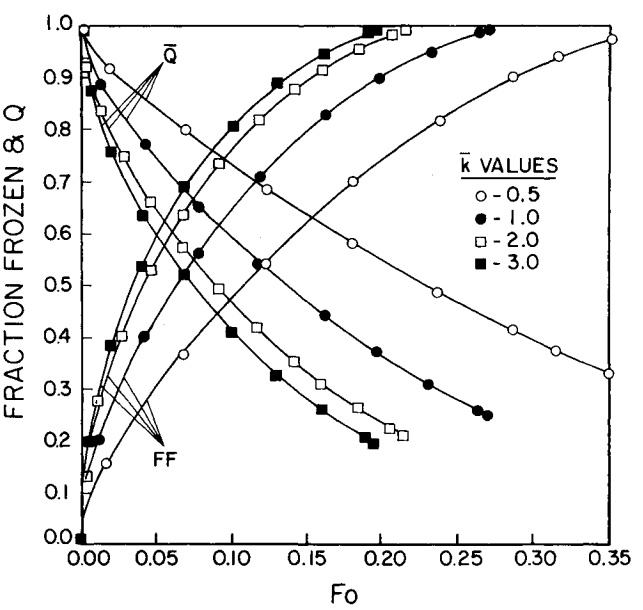


**Fig. 5 Effect of wall thermal conductivity on the freezing process.**

The baseline case represents a rather tall, thin cylinder ($\bar{G} = 0.1$). Figure 6 shows FF and $\bar{Q}$ results for other aspect ratio values. For a given radius $R$ (the length scale appearing in the Fourier number), changes in aspect ratio represent changes in container height. The shorter the container (larger $\bar{G}$), the more quickly freezing will occur, since the ratio of outer surface area to PCM volume becomes larger and larger. Note that for higher values of $\bar{G}$, waviness in the FF curves disappears, since a smaller vertical distance is being accommodated by an equal number of finite-difference nodes (40, in these cases).

Figure 7 shows four phase front profiles for different aspect ratio values. When $\bar{G} = 0.1$, radial propagation of the phase front dominates the freezing, while for larger $\bar{G}$ values, axial propagation plays a more significant role. Because the outer wall is maintained isothermal, freezing continues to completion.

A higher value of the Stefan number for the isothermal outer wall case (type I) represents a colder exterior boundary temperature and, hence, an increased freezing rate. This is evidenced in Fig. 8. The effects appear to be countered, however, by the wall thermal resistance, so that heat-transfer rates for *Ste* much greater than about 2 are not significantly increased.

The effect of varying wall thickness ($\bar{R}$, $\bar{Z}$) is shown in Fig. 9. The abscissa has been modified so that the length scale is the PCM radius rather than the outer cylinder radius, making a comparison physically meaningful. Both type I and type II external cooling conditions are shown in the figure; $\bar{Q}$ curves have been deleted for clarity. For the isothermal outer surface case, the external cooling dominates the heat-transfer process for the chosen wall thermal properties. There is not much difference between a thick and a thin wall, except for some retarding of solidification due to wall resistance. However, for an adiabatic outer wall, the "freezing capacity" is governed directly by the volume of the wall which is present, so that significant differences in freezing rates are evident. For thinner walls, an asymptotic frozen fraction may be observed. Figure 10 illustrates this effect further for the type II boundary condition.

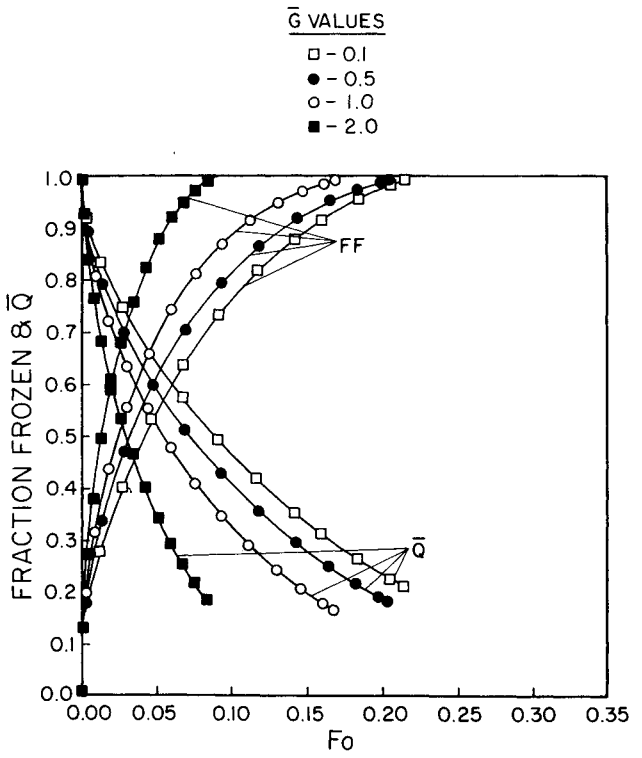


Fig. 6 Effects of container aspect ratio on the freezing process.

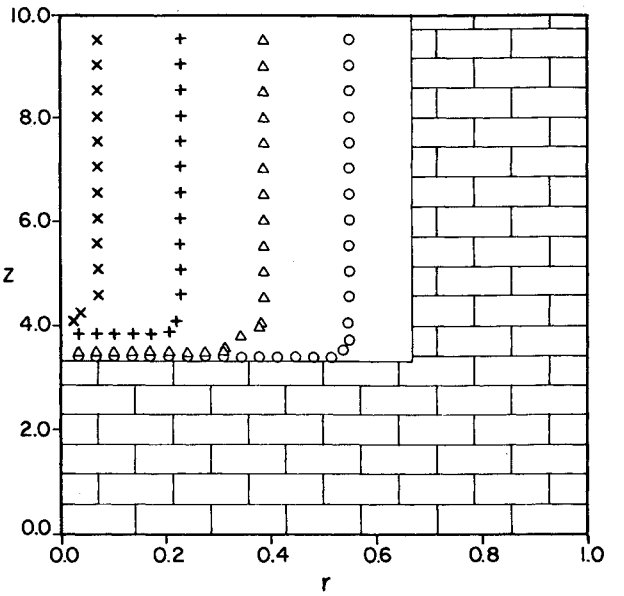


Fig. 7a Phase front profiles for baseline case, $\bar{G} = 0.1$.

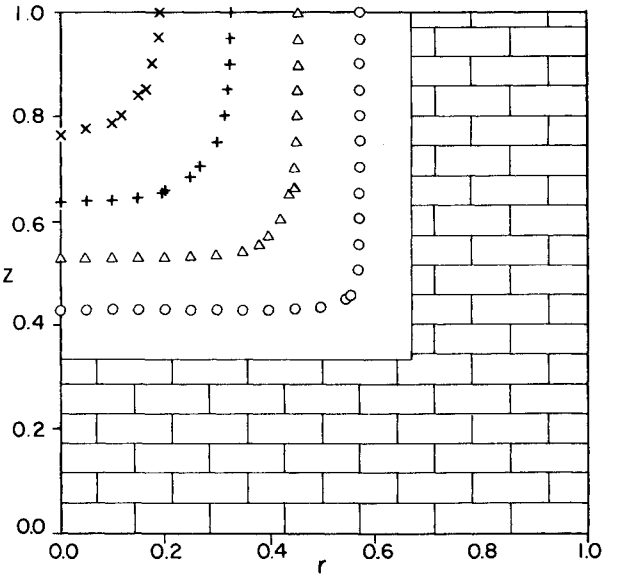


Fig. 7b Phase front profiles, $\bar{G} = 1.0$.

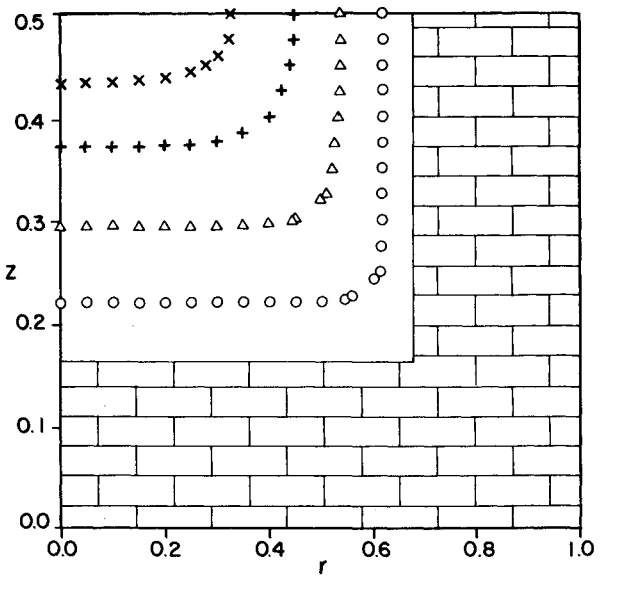


Fig. 7c Phase front profiles, $\bar{G} = 2.0$.

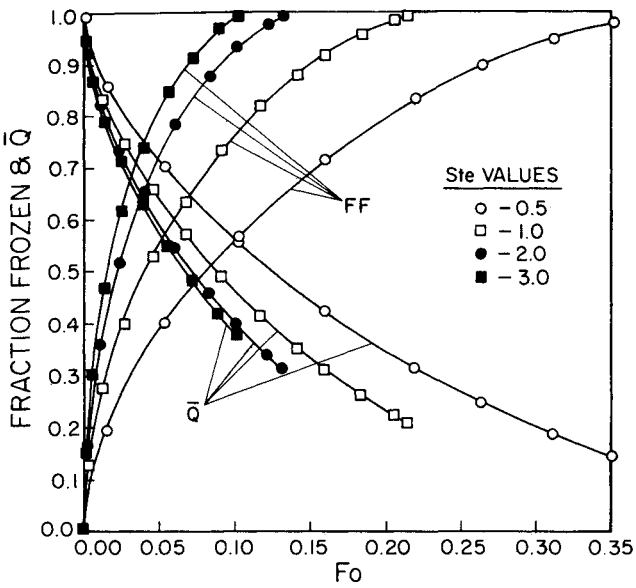


**Fig. 8 Effect of Stefan number on the freezing process, type I boundary condition.**

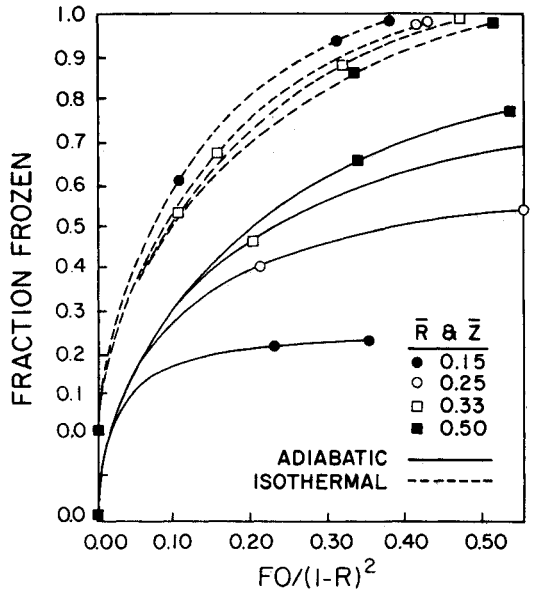


**Fig. 9 Effect of wall thickness on the freezing process: ----, type I boundary condition; ——, type II boundary condition.**

Figure 11 shows the effect of varying the thermal diffusivity ratio $\bar{\alpha}$, which, for equal values of $\bar{k}$, is equivalent to varying the wall heat capacity. For the isothermal outer wall condition, external cooling dominates the heat-transfer process and the wall heat capacity has little effect. However, for an adiabatic wall, the heat capacity of the wall is much more significant. Large values of $\bar{\alpha}$ imply a lower wall heat capacity, so that freezing rates are significantly reduced. Finally, the effects of initial wall temperature distribution are illustrated in Fig. 12. For the large aspect ratio baseline case, and for most other situations, the isothermal outer wall condition (type I) dominates over initial wall subcooling. If the wall is initially at the phase change temperature, then the onset of solidification is delayed slightly until the *inner* wall temperature is cooled. However, there is no other great difference. For an adiabatic outer wall, Fig. 12 shows a uniform subcooling initial condition with an initial wall gradient condition. As expected, freezing rates are severely retarded when a significant portion of the sidewall is near the phase change temperature.

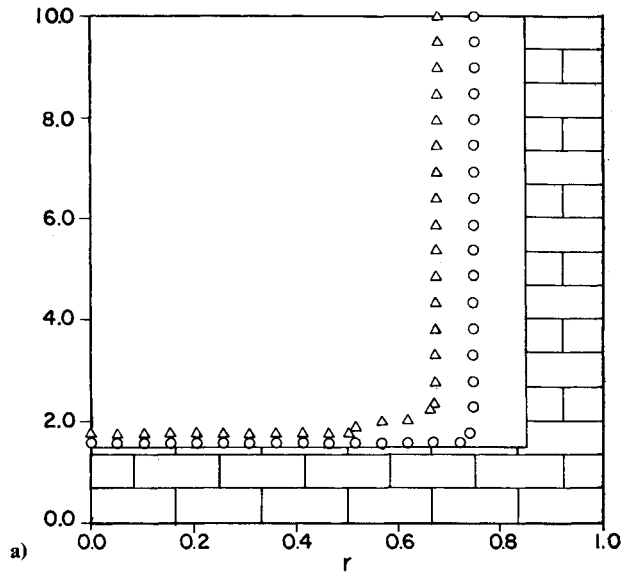


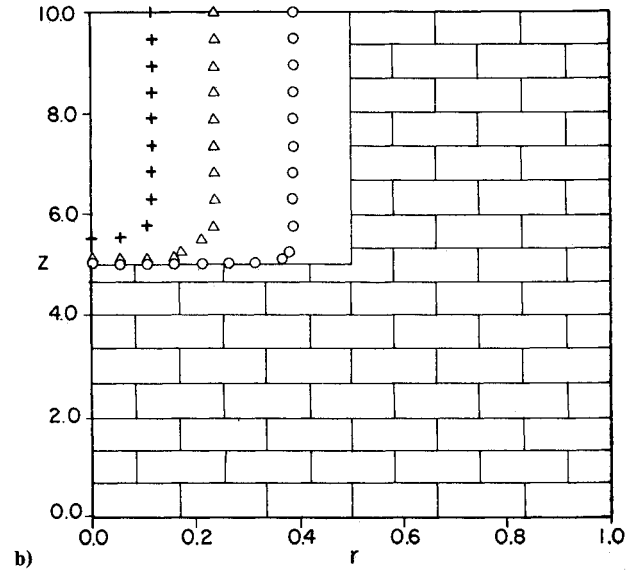


**Fig. 10 Effect of wall thickness on phase front profiles, type II boundary condition: a) $\bar{Z} = \bar{R} = 0.15$; b) $\bar{Z} = \bar{R} = 0.50$.**

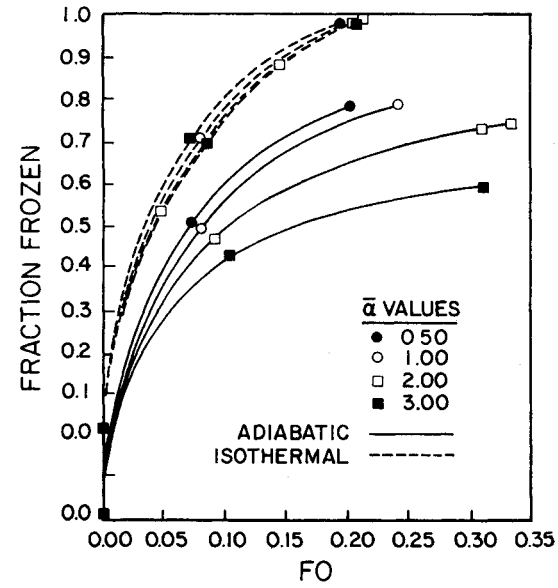


**Fig. 11 Effect of wall heat capacity on the freezing process: ----, type I boundary condition; ——, type II boundary condition.**

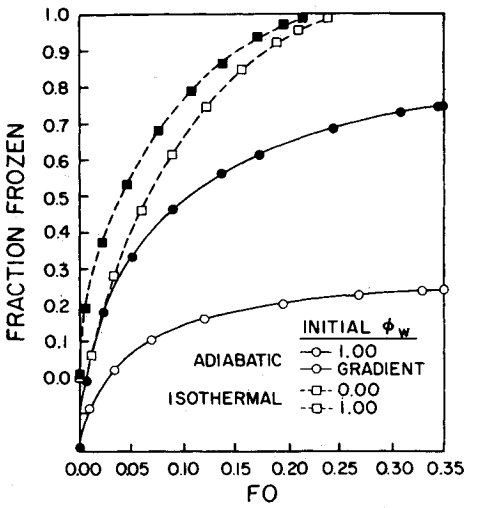


**Fig. 12 Effect of initial wall temperature distribution on the freezing process: ----, type I boundary condition; ——, type II boundary condition.**

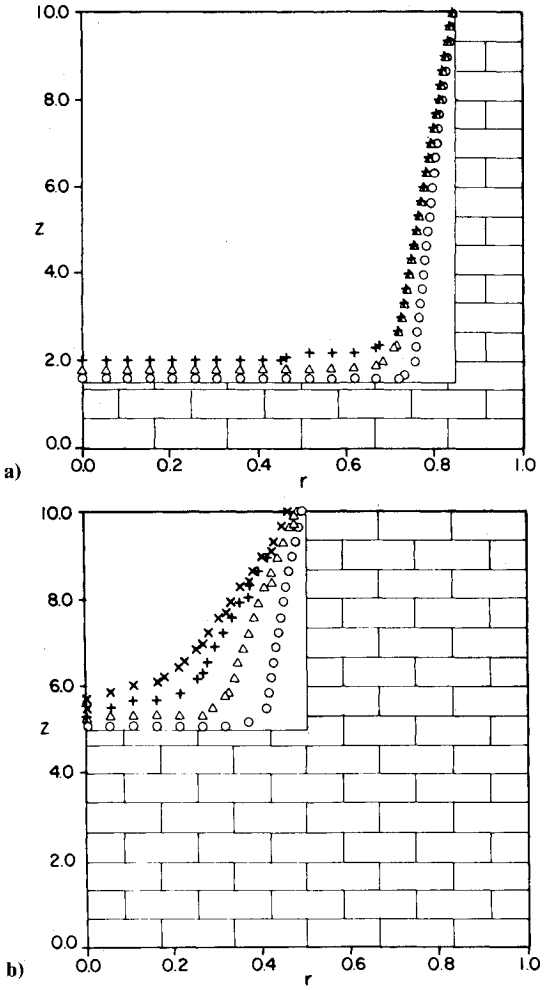


**Fig. 13 Phase front profiles with nonuniform initial wall temperature distribution, type II boundary condition: a) $\bar{R} = \bar{Z} = 0.15$; b) $\bar{R} = \bar{Z} = 0.50$.**

Phase front profiles for the gradient initial condition also demonstrate the retarding of solidification near the top of the container (Fig. 13). The slant in the phase front profile remains well into the freezing process, indicating that conduction along the sidewall is not an effective heat-transfer node.

## Summary

1) The principal conclusion of this study is that the thermal properties and initial temperature distribution of the container wall have the greatest effect on the solidification process when external cooling rates are low. The limiting cases of zero external cooling and isothermal outer wall were examined here.

2) There appear to be practical limits of external wall temperature for a given wall thermal resistance and wall thermal conductivity beyond which freezing rates are not enhanced.

3) A nonuniform initial wall temperature distribution has a significant effect on the local solid phase propagation rate.

## Acknowledgments

Support for the work reported herein was provided by the Martin Marietta Corporation through its membership in the Industrial Associates Program of the Center for Interactive Computer Graphics at Rensselaer Polytechnic Institute. Additional support in the final stages of the work was from National Science Foundation Grant MEA-8406402.

## References

[1]Wilson, D.G., Solomon, A.D., and Boggs, P.T. (eds.), *Moving Boundary Problems,* Academic Press, New York, 1978.

[2]Lunardini, V.J., *Heat Transfer in Cold Climates*, Van Nostrand Reinhold, New York, 1981.

[3]Viskanta, R., "Phase Change Heat Transfer," *Solar Heat Storage: Latent Heat Materials*, edited by G.A. Lane, CRC Press, Boca Raton, FL, 1983, pp. 153-222.

[4]Carslaw, H.S. and Jeager, J.C., *Conduction of Heat in Solids*, 2nd Ed., Clarendon Press, Oxford, 1959.

[5]Siegel, R. and Savino, J.M., "The Transient Solidification of a Flowing Liquid on a Cold Plate Including Heat Capacities of Frozen Layer and Plate," NASA TN-D-4353, 1968.

[6]Epstein, M., "The Growth and Decay of a Frozen Layer in Forced Flow," *International Journal of Heat and Mass Transfer*, Vol. 19, No. 11, 1976, pp. 1281-1288.

[7]El-Genk, M.S. and Cronenberg, A.W., "On the Thermal Stability of a Frozen Crust in Forced Flow on an Insulated Finite Plate," *International Journal of Heat and Mass Transfer*, Vol. 22, No. 12, 1979, pp. 1718-1723.

[8]El-Genk, M.S. and Cronenberg, A.W., "Stefan-like Problems in Finite Geometry," *Heat Transfer—San Diego 1979*, AIChE Symposium Series 189, Vol. 75, 1979, pp. 69-79.

[9]Shamsundar, N. and Sparrow, E.M., "Analysis of Multidimensional Conduction Phase Change via the Enthalpy Model," *Journal of Heat Transfer, Transactions of ASME*, Vol. 97, No. 3, 1975, pp. 333-340.

[10]Smith, R.N. and Koch, J.D., "Numerical Solution for Freezing Adjacent to a Finned Surface," *Proceedings of the 7th International Heat Transfer Conference*, Hemisphere Press, Washington, DC, Vol. 2, 1982, pp. 69-74.

[11]Boucheron, E.A. and Smith, R.N., "An Enthalpy Formulation of the SIMPLE Algorithm for Phase Change Heat Transfer Problems," ASME Paper 85-HT-7, 1985.

[12]Schneider, G.E., "A Numerical Study of Phase Change Energy Transport in Two-Dimensional Rectangular Enclosures," *Journal of Energy,* Vol. 7, July 1983, pp. 652-659.

[13]Sparrow, E.M. and Broadbent, J.A., "Freezing in a Vertical Tube," *Journal of Heat Transfer, Transactions of ASME*, Vol. 106, No. 1, 1983, pp. 217-225.

[14]Pike, R.L., "Numerical Analysis of Solidification in a Thick-Walled Cylindrical Enclosure," Center for Interactive Computer Graphics, Rensselaer Polytechnic Institute, Troy, NY, CICG Rept. TR-84021, 1984.

[15]Schneider, G.E. and Raw, M.J., "An Implicit Solution Procedure for Finite Difference Modeling of the Stefan Problem," *AIAA Journal,* Vol. 22, Nov. 1984, pp. 1685-1690.

[16]Peaceman, D.W. and Rachford, H.H., "The Numerical Solution of Parabolic and Elliptic Differential Equations," *Journal of the Society on Industrial and Applied Mathematics*, Vol. 3, 1955, p. 28.